Discovery of Acid-Stable Oxygen Evolution Catalysts : High-throughput Computational Screening of Equimolar Bimetallic Oxides

Seoin Back,[*,†] Kevin Tran,[‡] and Zachary W. Ulissi[*,‡]

†*Department of Chemical and Biomolecular Engineering, Sogang University, Seoul 04107, Republic of Korea*

‡*Department of Chemical Engineering, Carnegie Mellon University, Pittsburgh, Pennsylvania 15213, United States*

E-mail: sback@sogang.ac.kr; zulissi@andrew.cmu.edu

Abstract

Discovering acid-stable, cost-effective and active catalysts for oxygen evolution reaction (OER) is critical since this reaction is bottlenecking many electrochemical energy conversion systems. Current systems use extremely expensive iridium oxide catalysts. Identifying Ir-free or catalysts with reduced Ir-composition has been suggested as goals, but no systematic strategy to discover such catalysts has been reported. In this work, we performed high-throughput computational screening to investigate bimetalic oxide catalysts with space groups derived from those of IrO_x, identified promising OER catalysts predicted to satisfy all the desired properties: Co-Ir, Fe-Ir and Mo-Ir bimetallic oxides. We find that for the given crystal structures explored, it is essential to include noble metals to maintain the acid-stability, although one-to-one mixing of noble and non-noble metal oxides could keep the materials survive under the acidic conditions. Based on the calculated results, we provide insights to efficiently perform future high-throughput screening to discover catalysts with desirable properties.

Electrocatalysis plays an important role to effectively utilize renewable energy source derived electricity.[1] As the renewable energy sources are intermittent, it is desirable to store the produced electricity in the form of chemical bonding energies. In addition, energy efficient upgrading of low-value chemicals to value-added chemicals is also possible based on cathodic electrocatalytic reactions, such as N_2 reduction to NH_3 or CO_2 reduction to long-chain hydrocarbons or alcohols. H_2 fuel can also be generated electrochemically from H_2O to be used for fuel cell applications. For these catalytic reactions, the corresponding anode reaction is, in most cases, a four-electron H_2O oxidation to produce O_2 (O_2 evolution reaction, henceforth OER), which currently suffers from the lack of electrocatalysts with the desired properties.

To maximize the total efficiency of these electrochemical energy conversion systems, ideal catalysts for the anode reaction should satisfy the following criteria; stability in acidic reaction conditions, high activity and low cost. Acidic reaction conditions for the OER are preferred over alkaline conditions because of higher conductivity, current density, less parasitic reactions and the ability to use a cation exchange membrane.[2–5] Although many materials have been investigated for OER, only Ir and Ru based catalysts have shown state-of-the-art catalytic activity and stability under the acidic condition.[6] Recently, various Ru and Ir containing oxide materials have shown improved stability under the acidic condition and enhanced catalytic activity.[3,7–10]

In heterogeneous catalysis, atomic-level simulations have helped to significantly accelerate the catalyst discovery by constructing free energy diagrams of catalyst surfaces and predicting the theoretical overpotentials (η_{OER}), and suggesting materials with low η_{OER} for further experimental validations.[1] For various catalyst surfaces, scaling relations of binding energies have been reported, where binding energy of reaction intermediates interacting with catalyst surfaces through the same atomic elements could be represented by that of other reaction intermediates, for example, ΔG_{OH*} and ΔG_{OOH*} or ΔG_{N*} and ΔG_{NH_x*}.[11,12] The scaling relations could effectively reduce multi-dimensional reaction networks to one or two

dimensions, making it possible to estimate the catalytic activity based on simple calculations of binding energies of one or two reaction intermediates.[11] For example, ΔG_{OOH*} and ΔG_{OH*} are linearly correlated on oxide surfaces ($\Delta G_{OOH*} = \Delta G_{OH*} + 3.2$),[11] thus the OER overpotential could be obtained from DFT calculations of ΔG_{O*} and ΔG_{OH*} on the catalyst surfaces. Unfortunately, the conventional approach has only focused on the most stable facet and the scaling relation-based binding energies, although desired catalytic properties could come from the less stable facets and deviations from the scaling relations.[13,14] To overcome these limitations of the conventional approach, we recently reported more rigorous approach toward high-throughput calculations of oxides by considering various facets of oxides, reaction condition-relevant surface coverages and unique active sites.[13] We note that this concept was originally developed for inter-metallic alloys to discover catalysts for CO_2 electrochemical reduction.[15]

In this work, we develop an approach to discover acid-stable OER catalysts and we use this approach to perform high-throughput screening of equimolar bimetallic oxide catalysts. This is the first demonstration in the computational catalysis field to investigate a large collection of compositionally-diverse oxide crystal structures and facets as well as consider stability under the reaction condition. Potential equimolar crystal structures were formed from 8 crystal structures prototypes derived from IrO_x polymorphs[13] and bimetallic combinations of 26 transition metal elements, 2,600 in total. We evaluated the electrochemical stability of bimetallic oxides under the reaction conditions (pH=0 and E=1.23 V), which filtered out a majority of materials considered. For those combinations that are predicted to be stable, the most stable surface coverages and predicted OER catalytic activity are calculated. Crystal structures and calculation details are summarized in Figure 1 and Methods section (see **Supporting Information**). Based on these results we suggest a few Ir-based bimetallic oxides, including Co-Ir, Fe-Ir, and Mo-Ir combinations, that satisfy all the target properties and are predicted to outperform monometallic Ir oxides. Finally, we discuss technical details to more efficiently perform the high-throughput screening for future oxide

systems.

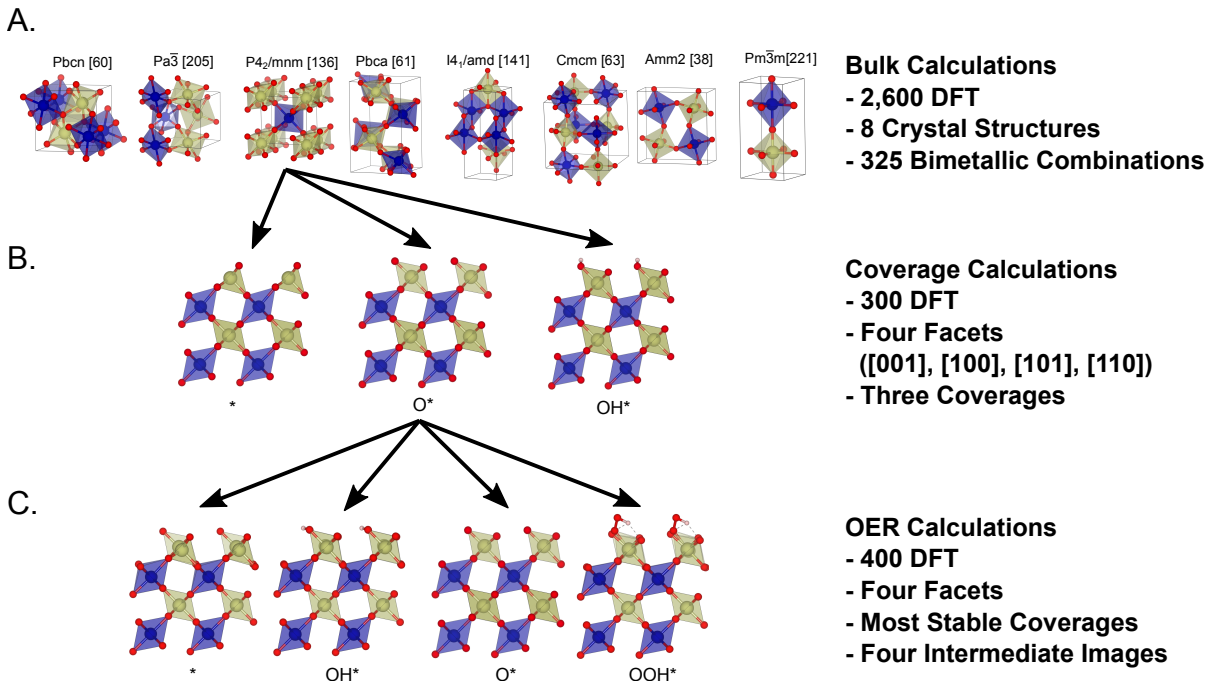

Figure 1: (A) All bulk crystal structures and space groups of bimetallic oxides investigated in this study. (B) Side views of example structures of coverage calculations: Bare surface (*), OH and O covered surfaces (OH*, O*). (C) Side views of example structures of OER calculations: Bare surface (*), OH, O, OOH adsorbed surfaces (OH*, O*, OOH*). Atomic cells of surface structures are doubled for a clear visualization.

To discover acid-stable OER catalysts, it is essential to evaluate their electrochemical stability under the reaction conditions. This is because many earth-abundant elements (Ni, Fe, Co, Mn) based catalysts have shown reasonable catalytic activities under the alkaline condition, but most of them were found to be unstable under the acidic condition.[6] They can either dissolve into the solution as ions, form more stable crystal structures or segregate into monometallic phases if they consist of multi-elements. Thus, we first evaluated the electrochemical stability ($\Delta G_{Pourbaix}$) of bimetallic oxides with respect to various phases of consisting elements including ions and solids. Figure 2A summarizes $\Delta G_{Pourbaix}$ of all combinations of bimetallic oxides, and only 14 out of 2,600 bimetallic combinations were predicted to be stable (< 0.1 eV/atom) under the acidic OER condition (Table S1). Further, a majority of stable combinations included Ir (Figure 2A), suggesting that Ir significantly contributes

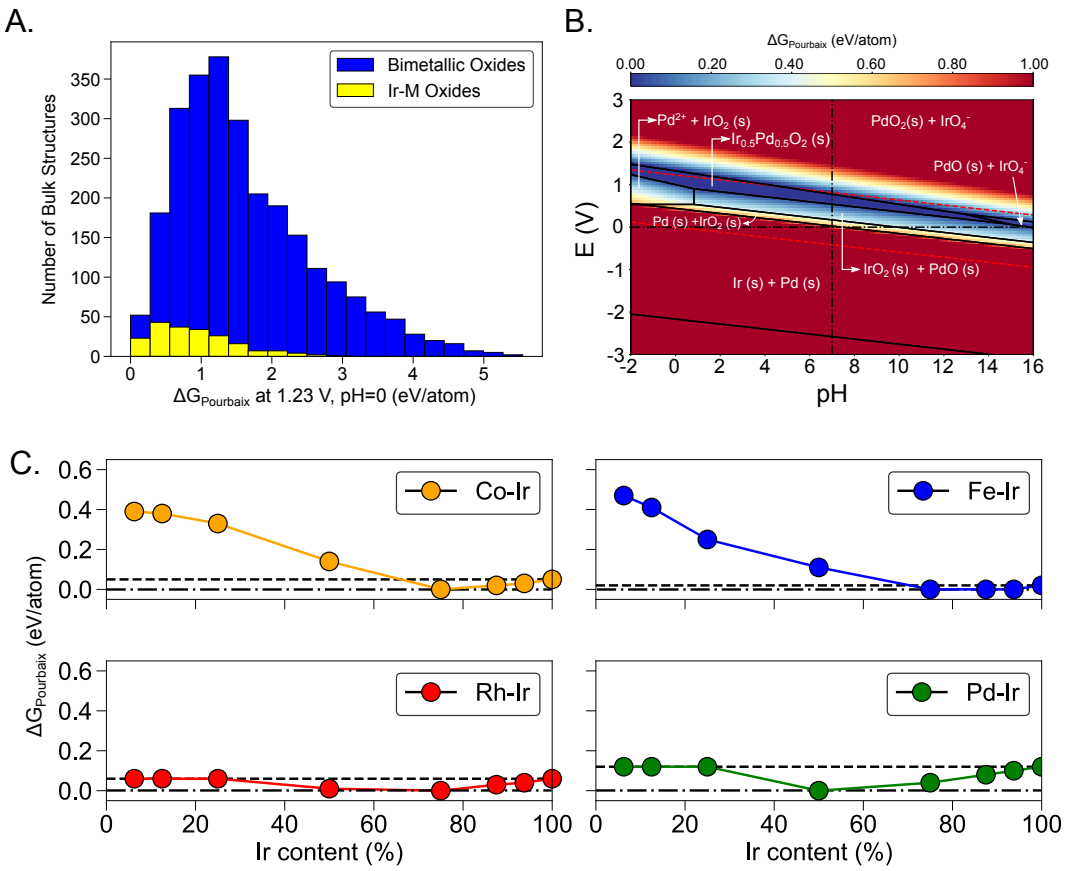

Figure 2: (A) Histogram of $\Delta G_{Pourbaix}$ for all bimetallic oxides (blue) and Ir containing oxides (yellow). (B) Computational Pourbaix diagram of Ir-Pd-O-H system. Free energy ($\Delta G_{Pourbaix}$) of rutile $Ir_{0.5}Pd_{0.5}O_2$ with respect to the most stable phase is illustrated as a color contour plot. The upper and lower red dashed lines correspond to the equilibrium potentials of O_2/H_2O (E^o = 1.23 V_{RHE}) and H^+/H_2 (E°=0.00 V_{RHE}), respectively. (C) $\Delta G_{Pourbaix}$ of Ir containing rutile bimetallic oxides with various ratios of M and Ir (M = Co, Fe, Rh, Pd). The stability of pure IrO_2 and the lowest stability ($\Delta G_{Pourbaix}$ = 0.0 eV) are plotted as a horizontal dashed and dash-dotted line for each combination, respectively. As $\Delta G_{Pourbaix}$ is calculated with respect to the most stable phase, we note that the relative stability of IrO_2 could differ for various bimetallic combinations.

to the stability. The Pourbaix diagram of one example combination, Pd-Ir, is illustrated in Figure 2B, and it visualizes the most stable phase at different pH and potential values and $\Delta G_{Pourbaix}$ of rutile bimetallic oxides ($Ir_{0.5}Pd_{0.5}O_2$) relative to the most stable phase. The Pourbaix diagrams of monometallic Ir and Pd show that the most stable phase at pH=0 and 1.23 V are IrO_2 and PdO_2, respectively,[16] but, when Ir and Pd are combined, $Ir_{0.5}Pd_{0.5}O_2$ becomes even more stable than their monometallic counterparts as can be found from the blue area in Figure 2B. Additionally, we investigated how metal composition affects the stability by varying metal-metal ratio and calculating the electrochemical stability (Figure 2C). Interestingly, bimetallic oxides are predicted to be destabilized once non-noble metals (Co, Fe) become dominant, while they remained stable for noble metal combinations regardless of the ratios considered. These results imply that it is essential to include noble metals to develop the acid-stable catalysts through the simple mixing approach for the given 8 crystal structures. We note, however, that more efficient approaches should be developed to investigate full composition and structural space, since our calculated results are limited to only small subsets of all possibilities.

To understand the effects of the crystal structures on the $\Delta G_{Pourbaix}$ for the given bimetallic combinations, we compared the relative $\Delta G_{Pourbaix}$ of different crystal structures. Figure 3 shows that the difference in $\Delta G_{Pourbaix}$ of oxides with the same oxidation states, *i.e.,* different structures within MO_2 or those within MO_3, is negligible compared to that between two different oxidation states, *i.e.,* MO_2 vs. MO_3, as can be found from a clear separation of blue (MO_2) and yellow (MO_3) symbols. Interestingly, Molybdenum (Mo) containing oxides energetically preferred higher oxidation states, MO_3, while other metal elements preferred MO_2 structures. We also plotted $\Delta G_{Pourbaix}$ of all Ir-based combinations in Figure S1 to understand the trend of oxidation states preference of transition metals. Early (Group 3, 4, 5) or late (Group 9, 10, 11, 12) transition metal containing systems generally preferred lower oxidation states probably due to fewer unpaired electrons compared to transition metals in the middle of the periodic table (Group 6, 7, 8). For bimetallic oxides containing Group 6,

7, 8 transition metals, multiple oxidation states have been observed to be stable[17,18] due to more unpaired electrons, making it possible to form higher oxidation states as in MO_3. For example, Mo with the electron configuration of [Kr] $4d^5$ $5s^1$ could be oxidized up to +6.

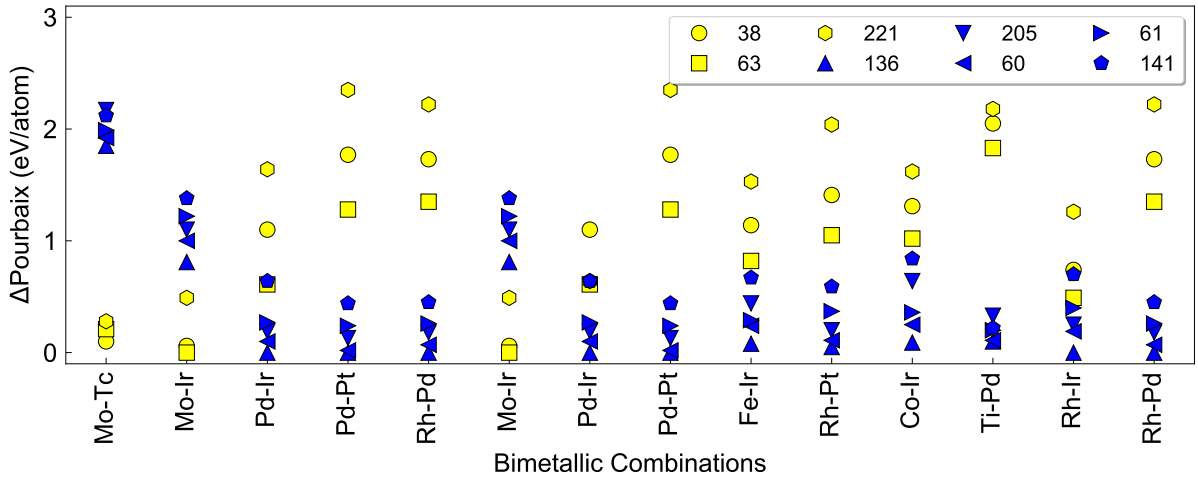

Figure 3: Relative electrochemical stability ($\Delta G_{Pourbaix}$) of different crystal structures of the bimetallic oxides at pH=0 and 1.23 V_{RHE}. Blue and yellow color indicates MO_2 and MO_3 polymorphs, respectively, and symbols correspond to crystal structures.

$$* + H_2O \leftrightarrow OH* + (H^+ + e^-) \tag{1a}$$

$$OH* \leftrightarrow O* + (H^+ + e^-) \tag{1b}$$

$$O* + H_2O \leftrightarrow OOH* + (H^+ + e^-) \tag{1c}$$

$$OOH* \leftrightarrow * + O_2 + (H^+ + e^-) \tag{1d}$$

For the 14 stable combinations, we calculated the η_{OER} to predict the catalytic activity of bimetallic oxides. We assumed four proton-electron coupled transfer mechanism[11] as shown in Eqn (1a) − (1d), and the η_{OER} is calculated as $\eta_{OER} = \max(\Delta G_{1a}, \Delta G_{1b}, \Delta G_{1c}, \Delta G_{1d})/e - 1.23$ V $= \max(\Delta G_{OH*}, \Delta G_{O*} - \Delta G_{OH}, \Delta G_{OOH*} - \Delta G_{O*}, 4.92 - \Delta G_{OOH*})/e - 1.23$ V. Four low-index facets ([001], [100], [101], [110]) were considered, the most stable coverages at the reaction condition were determined and all unique active sites considered.[13] Figure 4A shows the calculated η_{OER} and their active sites are plotted with different symbols. Various active

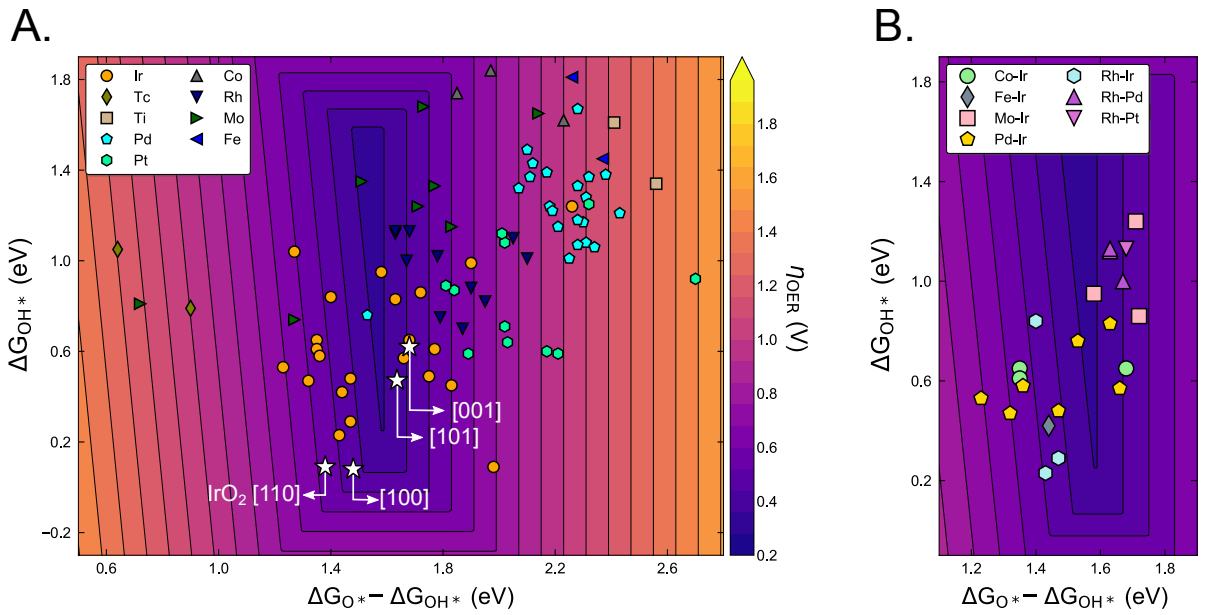

Figure 4: Two-dimensional volcano plot to predict η_{OER} of 14 acid-stable bimetallic oxides. The volcano plot was generated based on the scaling relation of $\Delta G_{OOH*} = 0.92\Delta G_{OH*} + 3.19$ (Figure S2). White stars indicate low-index facets of monometallic rutile IrO_2. Note that the volcano plot is slightly different from the one that we previously reported[13] due to the different slope of the scaling relation. This could be due to much larger and diverse collections of catalyst surfaces across many transition metal species. (A) All calculated sites were plotted, where symbols indicate surface active sites that interact with the reaction intermediates. (B) Only the promising candidates ($\eta_{OER} \leq 0.5$ V) are plotted, where symbols indicate bimetallic combinations instead of active sites as in (A).

sites, facets and bimetallic oxides were found to be as active as Ir-based catalysts with the η_{OER} smaller than 0.5 V. A majority of the active sites consist of Ir sites with a few Rh and Mo sites, and most of them are Ir based bimetallic oxides with the exception of Rh-Pd and Rh-Pt oxides. All promising candidates for acid-stable and active OER catalysis, and their detailed information is summarized in Table 1.

Table 1: Summary of the properties of the promising bimetallic oxide combinations for acid-stable and active OER catalysis. Only the combinations with η_{OER} equal to or less than 0.5 V are listed.

Combinations	Space group	$\Delta G_{Pourbaix}$ (pH=0, E=1.23 V_{RHE})	Facets	ΔG_{O*}	ΔG_{OH*}	ΔG_{OOH*}	Binding Site	η_{OER}
Pd, Ir	136	0.00	[001]	0.83	2.46	3.84	Ir	0.40
Pd, Ir	136	0.00	[100]	0.48	1.95	3.68	Ir	0.50
Pd, Ir	136	0.00	[110]	0.58	1.94	3.52	Ir	0.35
Pd, Ir	60	0.10	[001]	0.57	2.23	3.73	Ir	0.43
Pd, Ir	60	0.10	[100]	0.47	1.79	3.46	Ir	0.44
Pd, Ir	60	0.10	[101]	0.76	2.29	3.83	Pd	0.31
Pd, Ir	60	0.10	[110]	0.53	1.76	3.44	Ir	0.45
Mo, Ir	38	0.06	[001]	1.24	2.95	4.53	Mo	0.48
Mo, Ir	38	0.06	[001]	0.86	2.58	3.85	Ir	0.49
Mo, Ir	63	0.00	[001]	0.95	2.53	3.87	Ir	0.35
Mo, Ir	63	0.00	[101]	1.68	3.41	4.70	Mo	0.50
Rh, Ir	136	0.00	[001]	0.84	2.24	3.85	Ir	0.38
Rh, Ir	136	0.00	[100]	0.29	1.76	3.20	Ir	0.49
Rh, Ir	136	0.00	[110]	0.23	1.66	3.20	Ir	0.49
Rh, Pd	136	0.00	[100]	1.00	2.67	3.93	Rh	0.44
Rh, Pd	60	0.07	[100]	1.12	2.75	4.02	Rh	0.40
Rh, Pd	60	0.07	[110]	1.13	2.76	4.00	Rh	0.40
Co, Ir	136	0.09	[100]	0.65	2.00	3.62	Ir	0.39
Co, Ir	136	0.09	[101]	0.65	2.33	3.94	Ir	0.45
Co, Ir	136	0.09	[110]	0.61	1.96	3.62	Ir	0.43
Fe, Ir	136	0.08	[100]	0.42	1.86	3.52	Ir	0.43
Rh, Pt	136	0.05	[001]	1.13	2.81	4.05	Rh	0.45

Among these combinations, we found Co-Ir, Fe-Ir and Mo-Ir as promising candidates for further experimental validations. They are cost-effective than other noble metal based bimetallic combinations due to the low metal prices of Co, Fe and Mo (Table S2). Further, various facets ([100], [101], [110]) of Co-Ir with the space group 136 exhibited lower η_{OER} compared to IrO_2. More interestingly, Mo-Ir combination was found to be acid-stable in two different crystal structures (space group = 38, 63), where [001] facet of the space group 38, and [001] and [101] facets of the space group 63 were predicted to be very active for OER. Indeed, Co-Ir rutile bimetallic oxide synthesized through a selective leaching of Co from Co-

rich composite was reported to be acid-stable and more active than IrO_2 catalyst.[19] Other forms of Co-Ir bimetallic oxides were also reported to be OER active in alkaline[20] and neutral[21] conditions. Fe-Ir nanoparticles were prepared through a colloidal synthesis approach and exhibited the acid-stability and high catalytic activity.[22] The agreements between experimental results and these computational predictions reinforces the potential for catalyst discovery from high-throughput screening. In particular, Mo-Ir has not been reported in literature, thus this material is a promising candidate for experimental validation.

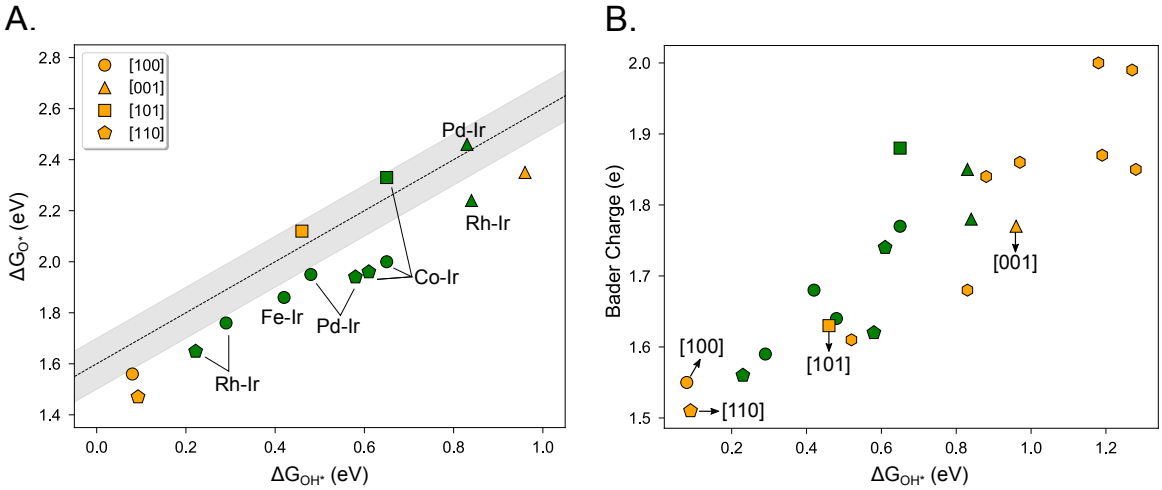

Figure 5: (A) ΔG_{O*} are plotted *versus* ΔG_{OH*} for rutile bimetallic oxides (green) and monometallic Ir oxides (orange). Symbols correspond to different low-index facets. The dashed black line indicates a target descriptor value ($\Delta G_{O*} - \Delta G_{OH*} = 1.6 \pm 0.1$ eV) to achieve low η_{OER} as shown in Figure 4, implying higher OER catalytic activity when closer to the target descriptor value. (B) Bader charges of surface Ir atoms are plotted *versus* ΔG_{OH*}. We additionally plotted Bader charges of surface Ir atom in monometallic Ir oxide of different crystal structures with orange hexagonal symbols taken from Ref.[13]

To understand the catalytic activities of the bimetallic oxides, we compared how energetics are affected by mixing two metal oxides. Since the observed high catalytic activities are mainly based on Ir sites, we focus on Ir-based rutile bimetallic oxides and compared with monometallic Ir oxide. As the origin of the activity improvement for specific bimetallic combinations is beyond the scope of this work, we limit the analysis to understand the overall trend. In Figure 5A, we plotted ΔG_{O*} *versus* ΔG_{OH*} of bimetallic and monometallic rutile Ir oxides, where $\Delta G_{O*} - \Delta G_{OH*} = 1.6$ is the optimal value to minimize the η_{OER}.,[11]

thus higher catalytic activity is expected when closer to the optimal descriptor value. As reported previously,[7,13] rutile IrO_2 [100] and [110] are found to bind the reaction intermediates too strongly, while [101] binds moderately and [001] binds weakly, again emphasizing the importance of exploring various facets as their binding strength toward reaction intermediates could substantially vary. In most cases, mixing with other transition metals weakened binding of O* and OH*, where the effects were as significant as 0.7 eV for ΔG_{OH*}, with the exception of [001]. The exception observed for [001] facet could be due to much smaller effect of mixing with other transition metals, where ΔG_{OH*} and ΔG_{O*} were affected by only 0.1 eV or less. Overall, all the sites are positioned very close to the optimal descriptor value to achieve lower η_{OER} compared to IrO_2. We further investigated the correlation between binding energies and oxidation states of Ir sites measured by Bader charge analysis[23] (Figure 5B). The trend is in agreement with the observation in the previous report[13] that higher oxidation states of surface Ir sites weakened interactions with the adsorbates. For active sites that bind reaction intermediates strongly or moderately ($\Delta G_{OH*} < 1.5$ eV), the scaling relation of ΔG_{O*} and ΔG_{OH*} ($\Delta G_{O*} = 1.47 \times \Delta G_{OH*} + 1.4$, Figure S3) overlaps well with the line ($\Delta G_{O*} - \Delta G_{OH*} = 1.6$) that corresponds to the optimal descriptor value, thus weakening of OH* and O* binding stayed close to the optimal descriptor value. This is also observed for promising active sites as all of them are positioned close to $\Delta G_{O*} - \Delta G_{OH*} = 1.6$ (black dashed line in Figure 5A). However, it is expected that too weakly binding sites ($\Delta G_{OH*} > 1.5$ eV) are less probable to become highly OER active sites because the slope difference between the two lines would result in significant deviations from $\Delta G_{O*} - \Delta G_{OH*} = 1.6$ eV. We note that ΔG_{O*} and ΔG_{OH*} have mainly been discussed since the scaling relation of ΔG_{OH*} and ΔG_{OOH*} ($\Delta G_{OOH*} = 0.92\Delta G_{OH*} + 3.19$, Figure S2) has been preserved for various facets and crystal structures of bimetallic oxides as also observed for surfaces of other metal oxides.[11] However, this, in turn, implies that the simple mixing approach could not achieve a breakthrough by deviating from the conventional scaling relation of ΔG_{OH*} and ΔG_{OOH*} on the oxide surfaces. This breakthrough could possibly be achieved by exter-

nal factors such as a nanoscopic confinement,[24] and we consider this approach is beyond our high-throughput screening approach at this current stage.

From the experiences that we have acquired during the high-throughput DFT calculations of oxides to discover OER catalysts, we suggest the following that could help other researchers in the field to more efficiently perform the high-throughput screening to discover catalysts with desired properties:

- As shown in Figure S2 and mentioned in the main text, the scaling relation of ΔG_{OH*} and ΔG_{OOH*} is well preserved for various crystal structures, bimetallic combinations and facets. Although this implies that there is little chance to break the scaling relation through the simple mixing approach, this in turn highlights that we can substantially reduce the use of computational resources by estimating ΔG_{OOH*} via the scaling relation with ΔG_{OH*}. This is because of more degrees of freedom of adsorbate configurations of OOH*, which makes geometry optimizations of OOH* adsorbed surfaces much more expensive and intricate compared to simpler adsorbates such as O* and OH*. Indeed, we spent a fair amount of computational resources to deal with H detachment from OOH* adsorbate.

- In Figure S4, we plotted ΔG_{X*} (X=O*, OH*) obtained from the coverage calculations ($\Delta G_{X*,cov}$) and OER calculations ($\Delta G_{X*,OER}$), where the coverage calculations result in the averaged binding free energies, while the OER calculations predict binding free energies of a single adsorbate at the specific active site for the given coverages. Thus, one $\Delta G_{X*,cov}$ calculation corresponds to two $\Delta G_{X*,OER}$ calculations as there could be two different metal sites on the surface for bimetallic oxides, while there is one-to-one correspondence for monometallic oxides. We observed a descent correlation between binding free energies calculated on the basis of two different references. These observations suggest that one can further reduce the number of DFT calculations by accurately predicting $\Delta G_{X*,OER}$ from $\Delta G_{X*,cov}$ through regression models or classifying promising/unpromising surfaces on the basis of $\Delta G_{O*,cov}$ and $\Delta G_{OH*,cov}$, then performing

further calculations only for the promising candidates. This will be the topic of the follow-up research.

In this work, we performed systematic high-throughput calculations to discover catalysts that could potentially replace the state-of-the-art Iridium oxide catalysts. This is the first approach in the computational catalysis field that considers various (1) bimetallic combinations, (2) crystal structures, (3) electrochemical stability under the acidic OER conditions, (4) several possible facets, (5) reaction condition-relevant surface coverages and (6) all unique active sites of oxide materials. Considering all the factors, we suggested Co-Ir, Fe-Ir and Mo-Ir bimetallic oxides as active, acid-stable and cost-effective OER catalysts, particularly Mo-Ir which has not been reported in literature. We expect our systematic approach to facilitate the discovery of promising oxide catalysts for various catalytic applications not limited to OER.

Acknowledgement

This research used resources of the National Energy Research Scientific Computing Center, a DOE Office of Science User Facility supported by the Office of Science of the U.S. Department of Energy under Contract No. DE-AC02-05CH11231.

Supporting Information Available

Relative electrochemical stabilities of different structures of Ir-based bimetallic oxides. Scaling relations between ΔG_{OOH*} and ΔG_{OH*}, and ΔG_{OH*} and ΔG_{O*}. Correlation between $\Delta G_{X*,cov}$ and $\Delta G_{X*,OER}$. A summary of bimetallic oxides that are predicted to be stable (0.1 eV/atom) under the acidic condition.

References

(1) Seh, Z. W.; Kibsgaard, J.; Dickens, C. F.; Chorkendorff, I.; Nørskov, J. K.; Jaramillo, T. F. Combining Theory and Experiment in Electrocatalysis: Insights into Materials Design. *Science* **2017**, *355*, eaad4998.

(2) Sardar, K.; Petrucco, E.; Hiley, C. I.; Sharman, J. D.; Wells, P. P.; Russell, A. E.; Kashtiban, R. J.; Sloan, J.; Walton, R. I. Water-Splitting Electrocatalysis in Acid Conditions Using Ruthenate-Iridate Pyrochlores. *Angew. Chem. Int. Ed.* **2014**, *53*, 10960–10964.

(3) Lin, Y.; Tian, Z.; Zhang, L.; Ma, J.; Jiang, Z.; Deibert, B. J.; Ge, R.; Chen, L. Chromium-Ruthenium Oxide Solid Solution Electrocatalyst for Highly Efficient Oxygen Evolution Reaction in Acidic Media. *Nat. Commun.* **2019**, *10*, 162.

(4) Carmo, M.; Fritz, D. L.; Mergel, J.; Stolten, D. A Comprehensive Review on PEM Water Electrolysis. *Int. J. Hydrog. Energy* **2013**, *38*, 4901–4934.

(5) Kim, Y.-T.; Lopes, P. P.; Park, S.-A.; Lee, A.-Y.; Lim, J.; Lee, H.; Back, S.; Jung, Y.; Danilovic, N.; Stamenkovic, V., et al. Balancing Activity, Stability and Conductivity of Nanoporous Core-Shell Iridium/Iridium Oxide Oxygen Evolution Catalysts. *Nat. Commun.* **2017**, *8*, 1449.

(6) McCrory, C. C.; Jung, S.; Peters, J. C.; Jaramillo, T. F. Benchmarking Heterogeneous Electrocatalysts for the Oxygen Evolution Reaction. *J. Am. Chem. Soc.* **2013**, *135*, 16977–16987.

(7) Strickler, A. L.; Flores, R. A.; King, L. A.; Nørskov, J. K.; Bajdich, M.; Jaramillo, T. F. Systematic Investigation of Iridium-Based Bimetallic Thin Film Catalysts for the Oxygen Evolution Reaction in Acidic Media. *ACS Appl. Mater. Interfaces* **2019**, *11*, 34059–34066.

(8) Feng, Q.; Zou, J.; Wang, Y.; Zhao, Z.; Williams, M. C.; Li, H.; Wang, H. Influence of Surface Oxygen Vacancies and Ruthenium Valence State on the Catalysis of Pyrochlore Oxides. *ACS Appl. Mater. Interfaces* **2020**,

(9) Strickler, A. L.; Higgins, D.; Jaramillo, T. F. Crystalline Strontium Iridate Particle Catalysts for Enhanced Oxygen Evolution in Acid. *ACS Appl. Energy Mater.* **2019**, *2*, 5490–5498.

(10) Seitz, L. C.; Dickens, C. F.; Nishio, K.; Hikita, Y.; Montoya, J.; Doyle, A.; Kirk, C.; Vojvodic, A.; Hwang, H. Y.; Nørskov, J. K., et al. A Highly Active and Stable $IrO_x/SrIrO_3$ Catalyst for the Oxygen Evolution Reaction. *Science* **2016**, *353*, 1011–1014.

(11) Man, I. C.; Su, H.-Y.; Calle-Vallejo, F.; Hansen, H. A.; Martinez, J. I.; Inoglu, N. G.; Kitchin, J.; Jaramillo, T. F.; Nørskov, J. K.; Rossmeisl, J. Universality in Oxygen Evolution Electrocatalysis on Oxide Surfaces. *ChemCatChem* **2011**, *3*, 1159–1165.

(12) Wang, S.; Petzold, V.; Tripkovic, V.; Kleis, J.; Howalt, J. G.; Skulason, E.; Fernandez, E.; Hvolbæk, B.; Jones, G.; Toftelund, A., et al. Universal Transition State Scaling Relations for (De)Hydrogenation over Transition Metals. *Phys. Chem. Chem. Phys.* **2011**, *13*, 20760–20765.

(13) Back, S.; Tran, K.; Ulissi, Z. W. Toward a Design of Active Oxygen Evolution Catalysts: Insights from Automated Density Functional Theory Calculations and Machine Learning. *ACS Catal.* **2019**, *9*, 7651–7659.

(14) Ulissi, Z. W.; Tang, M. T.; Xiao, J.; Liu, X.; Torelli, D. A.; Karamad, M.; Cummins, K.; Hahn, C.; Lewis, N. S.; Jaramillo, T. F., et al. Machine-Learning Methods Enable Exhaustive Searches for Active Bimetallic Facets and Reveal Active Site Motifs for CO_2 Reduction. *ACS Catal.* **2017**, *7*, 6600–6608.

(15) Tran, K.; Ulissi, Z. W. Active Learning across Intermetallics to Guide Discovery of Electrocatalysts for CO_2 Reduction and H_2 Evolution. *Nat. Catal.* **2018**, *1*, 696–703.

(16) Jain, A.; Ong, S. P.; Hautier, G.; Chen, W.; Richards, W. D.; Dacek, S.; Cholia, S.; Gunter, D.; Skinner, D.; Ceder, G.; Persson, K. Commentary: The Materials Project: A Materials Genome Approach to Accelerating Materials Innovation. *Apl Mater.* **2013**, *1*, 011002.

(17) Chen, Z.; Cummins, D.; Reinecke, B. N.; Clark, E.; Sunkara, M. K.; Jaramillo, T. F. Core–Shell MoO_3–MoS_2 Nanowires for Hydrogen Evolution: a Functional Design for Electrocatalytic Materials. *Nano Lett.* **2011**, *11*, 4168–4175.

(18) Ling, S.; Mei, D.; Gutowski, M. Reactivity of Hydrogen and Methanol on (0 0 1) Surfaces of WO_3, ReO_3, WO_3/ReO_3 and ReO_3/WO_3. *Catal. Today* **2011**, *165*, 41–48.

(19) Hu, W.; Zhong, H.; Liang, W.; Chen, S. Ir-Surface Enriched Porous Ir–Co Oxide Hierarchical Architecture for High Performance Water Oxidation in Acidic Media. *ACS Appl. Mater. Interfaces* **2014**, *6*, 12729–12736.

(20) Yu, A.; Lee, C.; Kim, M. H.; Lee, Y. Nanotubular Iridium–Cobalt Mixed Oxide Crystalline Architectures Inherited from Cobalt Oxide for Highly Efficient Oxygen Evolution Reaction Catalysis. *ACS Appl. Mater. Interfaces* **2017**, *9*, 35057–35066.

(21) Zhang, Y.; Wu, C.; Jiang, H.; Lin, Y.; Liu, H.; He, Q.; Chen, S.; Duan, T.; Song, L. Atomic Iridium Incorporated in Cobalt Hydroxide for Efficient Oxygen Evolution Catalysis in Neutral Electrolyte. *Adv. Mater.* **2018**, *30*, 1707522.

(22) Fu, L.; Cai, P.; Cheng, G.; Luo, W. Colloidal Synthesis of Iridium-Iron Nanoparticles for Electrocatalytic Oxygen Evolution. *Sustain. Energy Fuels* **2017**, *1*, 1199–1203.

(23) Tang, W.; Sanville, E.; Henkelman, G. A Grid-Based Bader Analysis Algorithm without Lattice Bias. *J. Phys. Condens. Matter* **2009**, *21*, 084204.

(24) Doyle, A. D.; Montoya, J. H.; Vojvodic, A. Improving Oxygen Electrochemistry through Nanoscopic Confinement. *ChemCatChem* **2015**, *7*, 738–742.

Graphical TOC Entry